Temperature and Salinity Variability in the SODA3, ECCO4r3, and ORAS5 Ocean Reanalyses, 1993–2015

JAMES A. CARTON, STEPHEN G. PENNY, AND EUGENIA KALNAY

Department of Atmospheric and Oceanic Science, University of Maryland, College Park, College Park, Maryland

(Manuscript received 16 September 2018, in final form 28 December 2018)

ABSTRACT

This study extends recent ocean reanalysis comparisons to explore improvements to several next-generation products, the Simple Ocean Data Assimilation, version 3 (SODA3); the Estimating the Circulation and Climate of the Ocean, version 4, release 3 (ECCO4r3); and the Ocean Reanalysis System 5 (ORAS5), during their 23-yr period of overlap (1993–2015). The three reanalyses share similar historical hydrographic data, but the forcings, forward models, estimation algorithms, and bias correction methods are different. The study begins by comparing the reanalyses to independent analyses of historical SST, heat, and salt content, as well as examining the analysis-minus-observation misfits. While the misfits are generally small, they still reveal some systematic biases that are not present in the reference Hadley Center EN4 objective analysis. We next explore global trends in temperature averaged into three depth intervals: 0–300, 300–1000, and 1000–2000 m. We find considerable similarity in the spatial structure of the trends and their distribution among different ocean basins; however, the trends in global averages do differ by 30%–40%, which implies an equivalent level of disagreement in net surface heating rates. ECCO4r3 is distinct in having quite weak warming trends while ORAS5 has stronger trends that are noticeable in the deeper layers. To examine the performance of the reanalyses in the Arctic we explore representation of Atlantic Water variability on the Atlantic side of the Arctic and upper-halocline freshwater storage on the Pacific side of the Arctic. These comparisons are encouraging for the application of ocean reanalyses to track ocean climate variability and change at high northern latitudes.

1. Introduction

Extensive surveys of ocean reanalyses in the past decade by the CLIVAR Global Synthesis and Observations Panel document the presence of biases in variables such as heat and salt storage, volume transports, sea level, and Atlantic meridional overturning circulation (Balmaseda et al. 2015; Karspeck et al. 2017; Palmer et al. 2017; Toyoda et al. 2017a,b; Shi et al. 2017; Storto et al. 2017; Valdivieso et al. 2017). Concern about these biases has caused these reanalyses to play more limited roles in studies such as those of the Intergovernmental Panel on Climate Change than their atmospheric counterparts (Rhein et al. 2013). Because several new-generation reanalyses have recently been released, this study explores the progress of ocean reanalyses through an examination of the bias and accuracy of temperature and salinity interannual to decadal variability during their 23-yr period of overlap, 1993–2015.

The first two reanalyses we consider—the Simple Ocean Data Assimilation, version 3 (SODA3; Carton et al. 2018a), and the European Centre for Medium-Range Weather Forecasts (ECMWF) Ocean Reanalysis System 5 (ORAS5; Zuo et al. 2018)—share similarities including 1/4° eddy-permitting horizontal resolution with a displaced North Pole or polar cap at high latitudes and a sequential algorithm to assimilate observations (SODA3 uses optimal interpolation with a 10-day assimilation cycle, while ORAS5 uses 3D-Var with a 5-day assimilation cycle). Both reanalyses assimilate SST observations as well as similar sets of subsurface temperature and salinity profiles. In the case of SODA3, the latter are obtained from the World Ocean Database 2013 (Smolyar and Zweng 2013), and in the case of ORAS5 they are obtained from the Met Office Hadley Center (Good et al. 2013). ORAS5 additionally assimilates

---

Corresponding author: James A. Carton, carton@atmos.umd.edu

satellite sea level and sea ice concentration data, and includes a constraint on SSS by nudging to climatology. Both reanalyses consist of multiple ensemble members.

The third reanalysis we consider is the Estimating the Circulation and Climate of the Ocean, version 4, release 3 (ECCO4r3; Forget et al. 2015; Fukumori et al. 2017). ECCO4r3 uses the MITgcm forecast model with enhanced resolution in the equatorial waveguide, relaxing to an approximately 100-km Mercator grid at higher latitudes, and also with a polar cap to avoid the convergence of meridians at the North Pole (Forget et al. 2015). Like ORAS5, ECCO4r3 uses an expanded set of observational constraints, including sea level, surface salinity, and time-dependent gravity. Most distinctively it employs 4D-Var in which the adjoint of the forecast model is combined with the forecast model itself to modify initial conditions, mixing parameters, and surface forcing fields (see Liang and Yu 2016) in such a way as to minimize the observation-minus-analysis misfits in a least squares sense subject to prescribed estimates of observation and forecast error. The cost function for ECCO4r3 also includes a penalty term minimizing the departure from the time mean climatology of temperature and salinity from the World Ocean Atlas 2009 (Boyer et al. 2009). ECCO4r3 uses the weekly $1° \times 1°$ gridded OISSTv2 SST analysis of Reynolds et al. (2002) and the monthly NASA microwave sea ice cover fraction analysis of Comiso (2000) as surface constraints. As a result of its design, the ECCO4 solution conserves ocean momentum, heat, and salt as represented on the nonlinear forecast model grid, subject to the various constraints described above.

We begin with an examination of the time-mean differences between the reanalyses and two gridded observation-based statistical objective analyses: OISSTv2 SST and the Met Office Hadley Center EN4.1.1 objective analysis of subsurface temperature and salinity. This is followed by an examination of the statistics of the monthly analysis-minus-observation misfits (after computing, the misfits are binned onto a regular grid for presentation here). Then we explore the temporal variability of temperature and salinity, including EN4.1.1 in this and subsequent comparisons. We believe that while EN4.1.1 is less accurate and has reduced variability than the ocean reanalyses since it lacks knowledge of dynamics such as geostrophy and wave dynamics, it is also should have reduced time mean bias because the historical climatology is built into its background estimate. We examine the two-decade trend in ocean warming by basin and globally, and the implied net surface flux expected as a result of Earth's top-of-the-atmosphere energy imbalance (Trenberth et al. 2016). Next, we examine interannual variability in the tropics to explore how the

reanalyses reproduce the strong tropical ocean interannual variability of water properties known to have occurred during our period of interest. Finally, we examine variability in the Nordic seas and Arctic, specifically focusing on the movement of Atlantic Water on the Atlantic side of the Arctic and freshwater storage in the Beaufort Sea on the Pacific side of the Arctic.

2. Data and methods

The primary datasets for this study are the 23 years of monthly reanalysis temperature and salinity fields spanning 1993–2015 as derived from SODA3, ECCO4r3, and ORAS5. All three reanalyses use ocean models with Mercator coordinate grids south of the Arctic, modified at high latitudes to avoid the convergence of meridians.

The four-member monthly SODA3 ensemble, which may be obtained from www.soda.umd.edu, differ from each other only in the applied forcing with one member forced by the NASA Modern-Era Retrospective Analysis for Research and Applications, version 2 (MERRA-2; Gelaro et al. 2017), a second by the ECMWF interim reanalysis (ERA-Interim; Dee et al. 2011), a third by the Japan Meteorological Agency 55-year Reanalysis (JRA-55; Kobayashi et al. 2015), and a fourth by the DRAKKAR (http://www.drakkar-ocean.eu/) Forcing Set 5.2 (DFS5.2; Dussin et al. 2016). For the first three of these forcing datasets, SODA3 uses a two-pass bias-correction procedure in which a seasonal heat and freshwater flux correction is calculated during a short 8-yr period analysis 2007–14 based on the analysis increments produced by the data assimilation (Carton et al. 2018b). The DFS5.2 forcing set has already undergone bias correction and so bias correction has not been applied to this dataset. SODA3 has a 50-level telescoping vertical grid with approximately 10-m resolution in the upper 100 m and has been remapped onto a regular $0.5° \times 0.5°$ Mercator horizontal grid using the Climate Data Operators of Schulzweida (2018) to perform bilinear interpolation (Zuo et al. 2019). The ensemble members are constructed using a sophisticated combination of perturbations to the observation values and positions, observation selection, as well as perturbations to surface fluxes with specified space and time scales (Zuo et al. 2017). The differences among the ensemble members are the result of variations in the choice of parameters such as mixing rates and observation errors. ORAS5 has 75 vertical levels with a much finer 1-m resolution near the surface, including 24 levels in the upper 100 m. The ORAS5 ensemble, which we obtained through the Copernicus Marine Service (http://marine.copernicus.eu) in October 2018, has already been

remapped onto a $1° \times 1°$ Mercator horizontal grid. For time series we present the estimates of the four-member (in the case of SODA3) or five-member (in the case of ORAS5) ensemble mean as well as the $\pm 1\sigma$ spread about the ensemble mean, computed by separately evaluating the ensemble mean and standard deviation as a function of time (in the case of time series). To the extent that the errors are Gaussian distributed, and if we were confident in our estimate of the ensemble standard deviation, then we should expect 68% of the true values to lie within these $\pm 1\sigma$ limits, increasing to 95% within $\pm 2\sigma$.

ECCO4r3 is also forced by ERA-Interim, and also applies a correction to the surface fluxes determined from the misfits to observations evaluated over the multidecadal optimization window. Monthly ECCO4r3 was downloaded from ftp://ecco.jpl.nasa.gov/Version4/Release3 in June 2018 already interpolated onto a $0.5° \times 0.5°$ grid horizontal grid with a 50-vertical-level grid similar to SODA3. One aspect of the comparison that can be affected by the details of regridding is the delicate relationship between temperature and salinity. In Fig. S1 in the online supplemental material we present the mean temperature–salinity relationships at fixed locations in three subtropical oceans, showing that the tightness of this relationship varies in among the analyses.

To evaluate monthly SST we compare temperature at the uppermost depth from each reanalysis to the OISSTv2 combined bulk SST analysis of Reynolds et al. (2002), downloaded from www.esrl.noaa.gov on July 2017. Reynolds et al. (2007) suggests that the random error in a revised version of the OISSTv2 analysis is as large as 0.6°C in the humid tropics, upwelling zones, and marginal ice zones, declining to less than 0.2°C in the dry subtropics. A comparison of OISSTv2 with an alternative OSTIA SST dataset (Donlon et al. 2012) is shown in Fig. S2 (top left). To evaluate upper-ocean temperature and salinity, we compare the reanalyses' averaged 0–300 m data to the monthly $1° \times 1° \times 42$-level Met Office EN4.1.1 objective analysis, which uses a "persistence forecast model," as a reference solution (Good et al. 2013). This analysis was downloaded from www.metoffice.gov.uk/hadobs in July 2017. The uncertainty estimates accompanying EN4.1.1, extensively discussed by Good et al. (2013), suggest that 100-m temperature and salinity are accurate to 0.5°–1°C and 0.07–0.5 psu, respectively. There are two versions of EN4.1.1. We choose the version of EN4.1.1 that has applied the Levitus et al. (2009) bathythermograph correction when comparisons are made to SODA3 and ECCO4r3, but use the alternative version with the bathythermograph correction of Gouretski and Reseghetti (2010) when comparing to ORAS5 to be consistent with the data used in that reanalysis. In Fig. S2 (bottom panels) we

show that the choice of different bathythermograph corrections introduces only a small time-mean change to 0–300-m temperature.

The comparisons described above are affected by the way EN4.1.1 fills data voids. To evaluate the bias and accuracy of the reanalyses only where observations are actually available we examine the analysis-minus-observation misfits for the 6.4 million temperature profiles and 3.8 million salinity profiles during 1993–2015, binned onto a uniform grid after differencing. The observation set we use to compute misfits was obtained from the World Ocean Database (WOD; Smolyar and Zweng 2013) standard level data and was downloaded from https://www.nodc.noaa.gov/OC5/WOD/pr_wod.html in June 2018. This dataset includes 1.5 million profiling float profiles (mainly Argo) and an additional 400 000 conductivity–temperature–depth casts. The WOD procedure for interpolation onto standard levels roughly follows the procedure of Reiniger and Ross (1968) and is described in detail in the World Ocean Database 2018 User's Manual (data.nodc.noaa.gov/woa/WOD/DOC/wodreadme.pdf). While ORAS5 assimilates profile data obtained from a separate source: the Hadley Center, a separate comparison of the two datasets shows only small ($\approx 5\%$) differences in included profiles (for that comparison the profiles are identified by their geographic location and time). The 900 000 bathythermographs included in the misfit examination were corrected following Levitus et al. (2009). The mean analysis minus observation differences help to identify biases in the analyses while the standard deviations of the misfits provide estimates of the weighted sum of observation and model forecast errors at the observation locations $[\sigma^2 \approx (\sigma_o^{-2} + \sigma_f^{-2})^{-1}$; Kalnay 2003].

Following the examination of misfits, we explore interannual to decadal variability of global and regional ocean heat content changes. For the tropics we limit our comparison to detection of changes in the volume of warm, >20°C water, which has been identified in previous studies such as Meinen and McPhaden (2001) as the layer where the thermal memory associated with tropical air–sea interactions reside. For the Arctic Ocean we begin by comparing time-mean reanalysis climatologies to the widely referenced $1° \times 1°$ monthly gridded temperature and salinity Polar Science Center Hydrographic Climatology version 3 (PHC3.0; Steele et al. 2001), downloaded from psc.apl.washington.edu/nonwp_projects/PHC in September 2017). PHC3.0 is based on the archive of observations primarily from the 1950s through the 1980s and so may have a somewhat cool climatology. We then examine changes in water properties in the well-sampled Greenland, Iceland, and Norwegian Seas as well as the changing temperature of
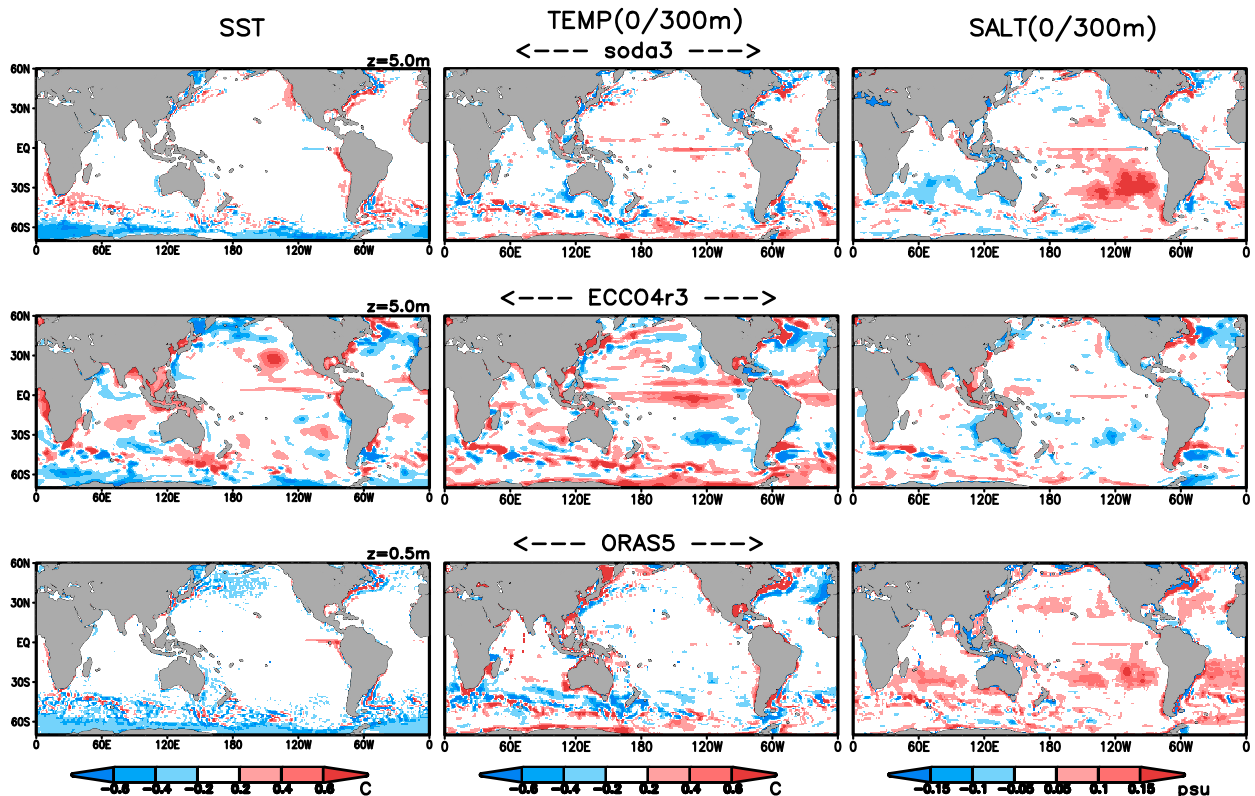
FIG. 1. Mean monthly difference (left) between uppermost-level temperature and OISSTv2 (°C) and (center) between 0–300-m temperature (°C) and (right) 0–300 salinity (psu) and EN4.1.1 during 1993–2015. For the comparison to (top) SODA3 and (middle) ECCO4r3 EN4.1.1 has been corrected using Levitus et al. (2009), while for the comparison to (bottom) ORAS5 EN4.1.1 has been corrected using Gouretski and Reseghetti (2010). The corresponding standard deviations for the left and center columns are given in Fig. S3.

the water spilling into the Barents Sea (Matishov et al. 2009; Boitsov et al. 2012). A goal of these comparisons is to explore the penetration of Atlantic Water into the Arctic and its transport through Fram Strait and the Barents Sea. To explore the changing freshwater storage on the Pacific side of the Arctic we compare the reanalyses to the observation-based storage estimates of Proshutinsky et al. (2009) in the Beaufort Gyre.

3. Results

The first part of the results section focuses on comparisons to observational analyses and the observations themselves. The second part examines how interannual to decadal variability is represented.

a. Comparison to observational analyses

We begin by comparing the shallowest available analysis level temperature to the OISSTv2 bulk SST objective analysis (Fig. 1, left). Reynolds et al. (2002)

report that the time-average difference between OISSTv2 and shipboard SST observations is < 0.25°C and so we choose ±0.3°C as the minimum contour interval for this comparison (although larger errors occur regionally, as noted in section 2). Relative to OISSTv2, SODA3 surface temperature shows a slight (<0.2°C) warm tendency, which grows to ~0.2°C in some of the eastern coastal upwelling zones. A similar pattern is evident in comparison to EN4.1.1 0–300-m temperature (Fig. 1, top-center panel). The low time-mean difference evident in the subtropical gyres is also representative of any given year (Fig. 2 shows time series of 0–300-m temperature difference in the North Pacific). ECCO4r3, which uses OISSTv2 as one of its constraints, is also warmer than OISSTv2, with larger, >0.2°C differences in the shallow seas surrounding Australasia, the South China Sea, the Sea of Okhotsk, and the Labrador Sea and in a small region of the eastern North Pacific near 30°N, 150°W. It also shows time-mean differences relative to EN4.1.1 0–300-m temperature.
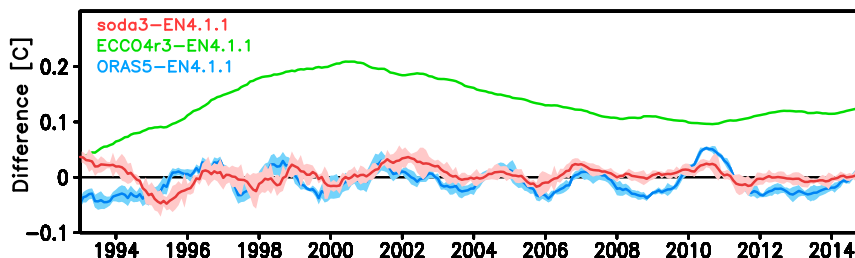
FIG. 2. Time series (1993–2015) of 0–300-m temperature difference from EN4.1.1 averaged across the central North Pacific (15°–60°N, 160°E–120°W). For the comparison to SODA3 and ECCO4r3, EN4.1.1 has been corrected using Levitus et al. (2009). For the comparison to ORAS5, EN4.1.1 has been corrected using Gouretski and Reseghetti (2010). Time series have been smoothed with a 1-yr running filter. Also, the $\pm 1\sigma$ ensemble spreads are indicated in lighter shades.

ORAS5, which assimilates surface temperature observations from a different, somewhat cooler, data source (Fig. S2), is slightly cooler than OISSTv2 (Fig. 1, bottom left). Both SODA3 and ORAS5 are cooler than OISSTv2 at deep southern latitudes. Despite these systematic differences the monthly variability of the SST differences for all three reanalyses are similarly less than 0.25°C in the subtropical gyres, rising to 0.25°–0.5°C in the higher eddy regions of the western basins and the Southern Ocean (Fig. S3). The standard deviations of the differences for all three reanalyses, defined as the square root of the mean square anomalies as a function of geographic position, fall within a ± 0.5°C monthly observation uncertainty reported by the SST observational analyses.

Finally we compare time-mean salinity 0–300 m with the corresponding estimates from EN4.1.1 (Fig. 1, right). ECCO4r3 shows quite close agreement with EN4.1.1. SODA3 is > 0.1 psu saltier than EN4.1.1 in the southeast Pacific Ocean on the eastern side of the subtropical South Pacific high surface salinity pool. This salinity difference only exists in the years prior to the enhanced data coverage of the early 2000s. In these low data years the South Pacific high surface salinity pool as represented in SODA3 and to a lesser extent ORAS5 extends several hundred kilometers too far eastward into the region where South Pacific Eastern Subtropical Mode Water is known to form (Wong and Johnson 2003).

b. Analysis minus observation misfits

We next examine the time average and standard deviations of the depth-averaged temperature and salinity misfits to the profile dataset in the upper 300 m, now including the EN4.1.1 analysis as well (Figs. 3 and 4). For the ensemble reanalyses we display the misfit of the ensemble mean. The time-mean EN4.1.1 misfits are small as expected, while SODA3 and ORAS5 also have generally small time-mean misfits (Figs. 3 and 4, left panels). There is no large surface salinity misfit in the

southeast subtropical Pacific in contrast to the anomaly that appeared in Fig. 1 (right panels) because the region was so poorly sampled. ECCO4r3 is too cool and fresh in the southern subtropics and too warm and salty in the deep tropics and the northern midlatitudes (Figs. 3 and 4, left panels). The standard deviations of temperature and salinity misfits for the three reanalyses are elevated in regions of high eddy activity (~0.6°C and 0.1 psu away from high eddy regions) and slightly larger than for EN4.1.1 (Figs. 3 and 4, right panels). SODA3 and ORAS5 also have somewhat higher standard deviations of temperature misfits in the tropical Atlantic.

The dramatic changes in the ocean observing system caused by the introduction of Argo observations in the early 2000s raise the question of the extent to which our analysis in Figs. 3 and 4 is dominated by the performance of the reanalyses in recent years. Figure 5 shows the time series of the standard deviation of the 0–300-m misfits averaged over three subtropical regions. For the two ensemble reanalyses the calculation is repeated separately for each ensemble member and the standard deviation of the ensemble members is used to estimate the $\pm 1\sigma$ monthly spread of the standard deviation of the misfits. EN4.1.1 always has the lowest levels of the standard deviation of misfits in all regions for both temperature (approximately 0.4°C) and salinity (approximately 0.04–0.06 psu). Some of the year-to-year variations in standard deviations of misfits can be tied to climate variability such as in the Pacific during El Niño years. The causes of other variations have not been determined. ECCO4r3 and ORAS5 have higher levels of the standard deviation of misfits than EN4.1.1, while SODA3 is generally in between the two. Changes in the spread of the standard deviation of the misfits are tied to the availability of observations and thus are particularly large for salinity prior to the deployment of Argo.

In recent years a number of studies have estimated the multidecadal warming rate of the global ocean based on
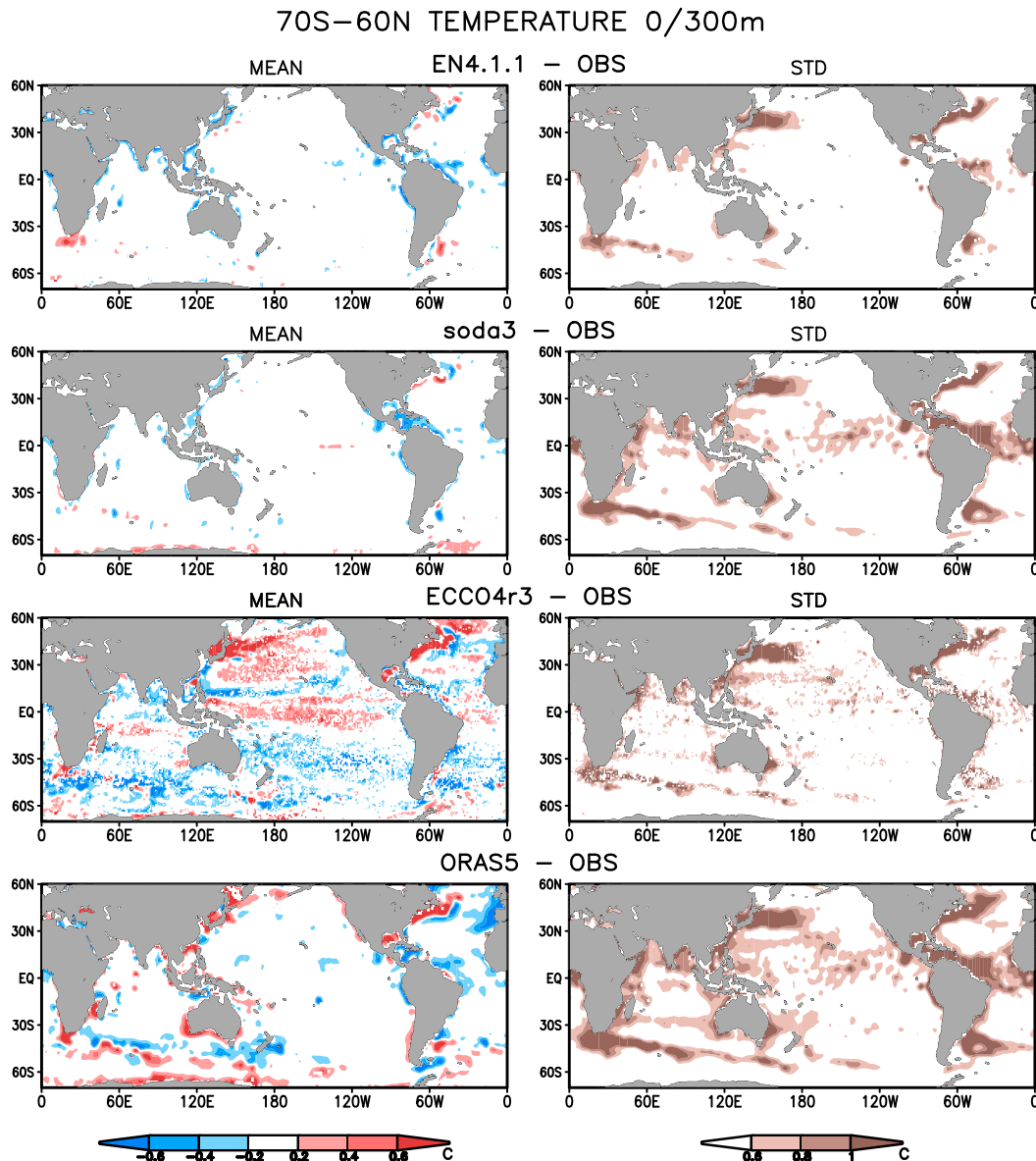
FIG. 3. Statistics of the monthly analysis minus observation potential temperature misfits (°C) averaged over 0–300 m: (left) 23-yr mean and (right) standard deviation.

gridded analyses of the temperature profile dataset (e.g., Domingues et al. 2008; Lyman and Johnson 2014). Recent studies give estimates in the range of $0.08°$–$0.10°\mathrm{C}\,(10\,\mathrm{yr})^{-1}$ in the upper 300 m, a rate similar to what we find for EN4.1.1 (Fig. 6). Multiplying this rate by the 300-m-layer thickness and the specific heat of seawater gives an estimate of the contribution of this 300-m layer to the surface energy imbalance over the ocean of 0.25–0.3 W m^{-2}. Previous attempts to estimate this same global net heat flux imbalance using ocean reanalysis temperatures have shown a discouragingly wide spread in estimates (Palmer et al. 2017, their Fig. 9).

Among the three reanalyses considered here, SODA3 provides a warming rate similar to EN4.1.1 and the other gridded analyses $[0.92 \pm 0.001°\mathrm{C}\,(10\,\mathrm{yr})^{-1}]$, while ORAS5 has a stronger warming rate $[0.130 \pm 0.003°\mathrm{C}\,(10\,\mathrm{yr})^{-1}]$ and ECCO4r3 has a much weaker warming rate $[0.037°\mathrm{C}\,(10\,\mathrm{yr})^{-1}]$ (Fig. 6). For the two ensemble reanalyses the uncertainty in the trend estimates, estimated by repeating the trend calculation on the individual ensemble members, is much smaller than the differences between the estimates, suggesting that the ensembles are underestimating the true uncertainties. For the deeper 300–1000-m layer EN4.1.1 and SODA3
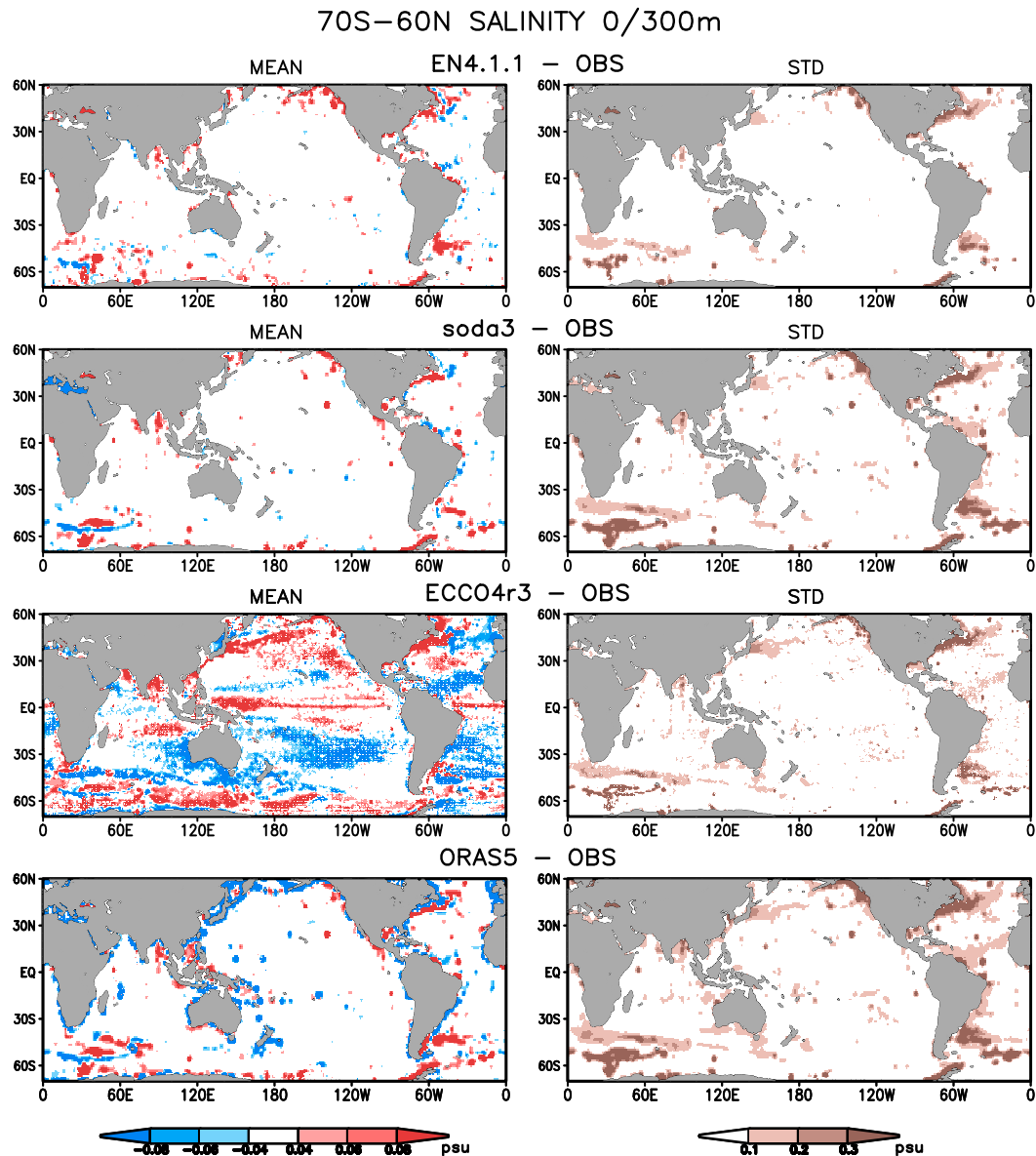
70S−60N SALINITY 0/300m

FIG. 4. Statistics of the monthly reanalysis minus observation salinity misfits (psu) averaged over 0–300 m: (left) 23-yr mean and (right) standard deviation.

again have warming rates similar to each other, both absorbing an additional 0.25 W m^{-2}, while ECCO4r3 absorbs little heat and ORAS5 absorbs nearly twice as much as EN4.1.1. A more detailed analysis of the heat uptake in SODA3 is provided in a separate study (J. Carton and T. Boyer 2018, unpublished manuscript).

The rate of ocean heat uptake varies geographically due to changes in cloud cover and turbulent fluxes. In Fig. 7 we explore those variations for the upper 300 m (the corresponding picture for the 300–1000-m layer is shown in Fig. S5). The Pacific gradually warms throughout our period of interest with dips in heat storage in El Niño years.

In the Atlantic much of the warming occurred during a 7-yr period (2000–06) during which the layer warmed by 0.1°–0.2°C. In contrast, the Indian Ocean began a period of dramatic warming after 2006 following (and likely a consequence of) the warming of the west Pacific (Han et al. 2014; Nieves et al. 2015; Lee et al. 2015). Interestingly ECCO4r3 does not capture this rapid warming of the Indian Ocean. Finally, heat content in the upper 300 m of the Southern Ocean remains fairly constant in all analyses during our period of interest, while the wide spread of the ensemble estimates indicates substantial uncertainties until the increase in observational sampling in the 2000s.
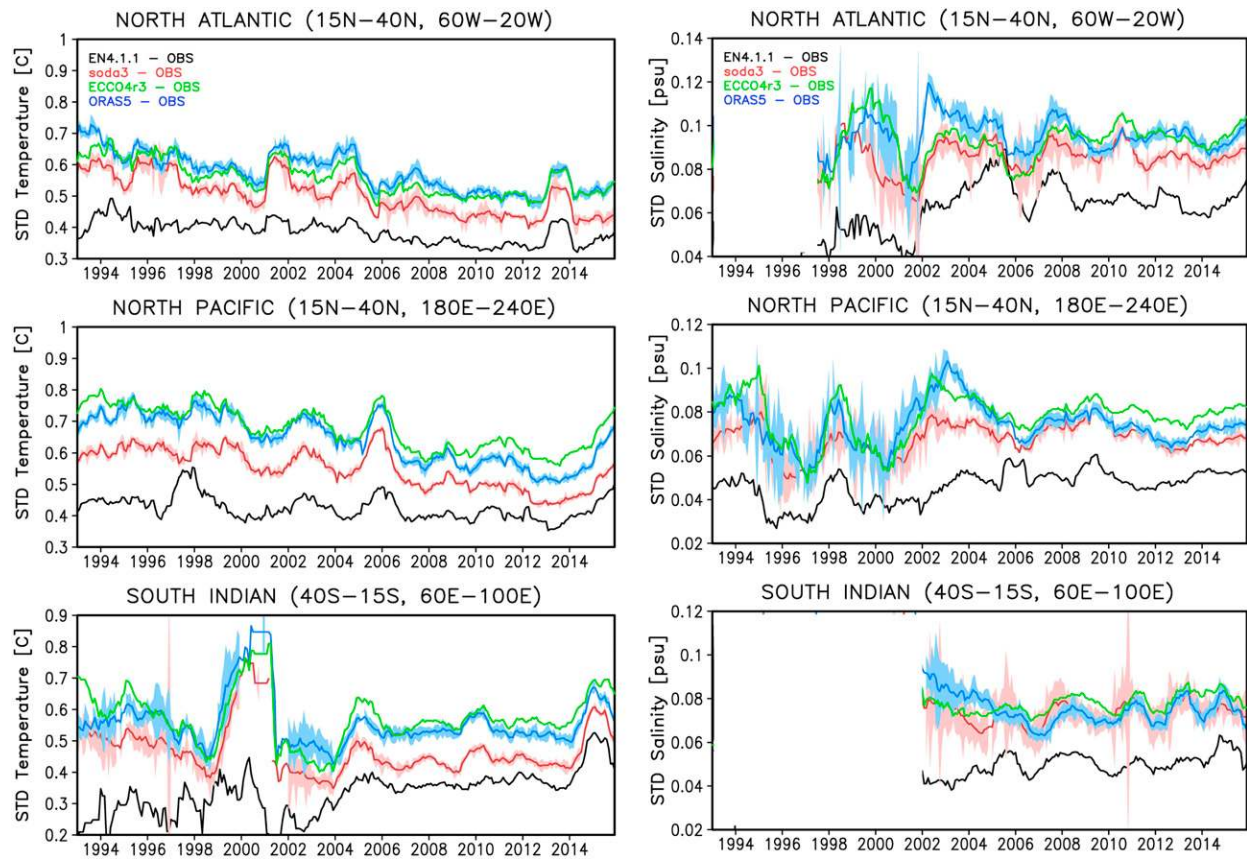
FIG. 5. Time series of annual average of the standard deviation of monthly 0–300-m analysis minus observation for (left) temperature and (right) salinity differences averaged over three subtropical domains in the (top) North Atlantic, (middle) North Pacific, and (bottom) south Indian Oceans. Light colors show the monthly $\pm 1\sigma$ spread of ensemble estimates.

The geographic differences of the 0–300-m temperature trends are also evident in the spatial maps of trend shown in Fig. 8. In all analyses the warming in the upper 300 m is concentrated in several geographic regions: the western side of the Pacific, the southern subtropical Indian Ocean, and the North Atlantic. In contrast, the upper 300 m of the eastern Pacific has been cooling as a result of anomalously strong trade winds in this basin beginning in the late 1990s (Carton et al. 2005; Nieves et al. 2015). The 300–1000-m layer is also warming throughout the Atlantic and the Southern Ocean layer but at 1/4 the rate of the 0–300-m layer (Fig. 8, center column). In the 1000–2000-m layer, all analyses show warming in the Atlantic (although ECCO4r3 shows cooling in the northern subtropics) and all show warming in the Southern Ocean in this layer (Fig. 8, right column).

In summary, SODA3 has heating rates generally similar to EN4.1.1 in multiple depth ranges while the ECCO4r3 heating rates are lower and ORAS5 heating rates are higher, but mostly with similar patterns. The similarity of SODA3 and EN4.1.1 may indicate that the

observations place a particularly strong constraint on this reanalysis relative to the model background estimates. We speculate that the lower ECCO4r3 heating rate in the Indian Ocean may be affected by differences in the rate of warm water entering the Indian Ocean from the western Pacific, while the high ORAS5 heating rates may be affected by the assimilation of sea level observations (since the assimilation of sea level is something that differs between ORAS5 and SODA3).

c. Tropics

Two strong El Niño events (1997/98 and 2015) and four strong La Niña events (1998/99, 1999/2000, 2007/08, 2010/11) dominate variability in the upper layers of the tropical Pacific Ocean during our period of interest. The most notable consequence of these events is the remarkable 30-m change in the depth of the warm water thickness in the central basin [defined following Meinen and McPhaden (2001)] in the shift from the El Niño conditions of 1997/98 to the La Niña conditions the following year (Fig. 9, top panel). The annual reanalysis warm water thicknesses generally agree to within 2 m of
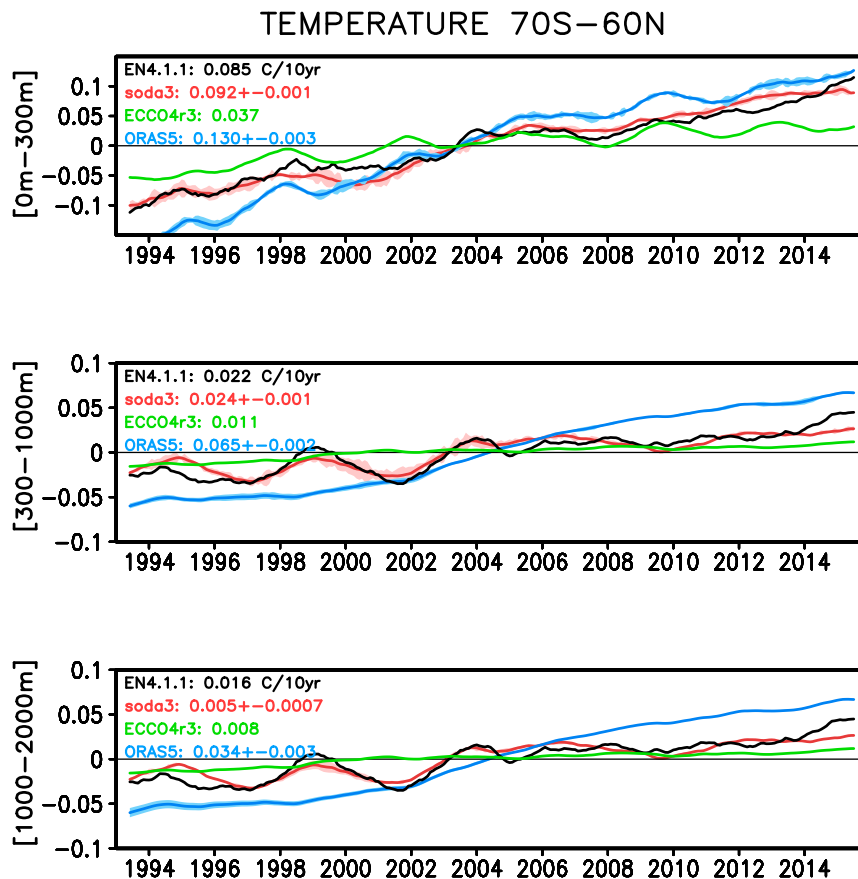
TEMPERATURE 70S-60N

FIG. 6. Time series of global (70°S–60°N) potential temperature anomalies (°C) from their 1993–2015 means in three depth ranges: (top) 0–300 m, (middle) 300–1000 m, and (bottom) 1000–2000 m. Time series have been smoothed with a running 2-yr filter. Linear trends are shown with ±1σ uncertainty estimates. The ±1σ ensemble spreads are indicated in lighter shades.

the EN4.1.1 thickness in this basin (basin definitions are shown in Fig. S4).

The Indian Ocean is also subject to climate variability (e.g., Saji et al. 1999) involving dipole-like zonal shifts of warm equatorial water associated with changes in the strength of the trade winds in the Indian Ocean. Positive Indian Ocean dipole events associated with strengthening trades and cool eastern Indian Ocean SSTs occurred in 1994, the second half of 1997, 2007, 2011/12, and 2015 whereas negative events occurred in 1996 and 1998. In Fig. 9 (middle panel) we present a time series of the warm water thickness in the central Indian Ocean defined analogous to the definition for the Pacific. As in the case of the Pacific, a striking feature of the time series for the central Indian Ocean basin is the dramatic shift in the depth of the thermocline between 1996 and 1998. In this basin the reanalysis monthly thickness estimates differ from EN4.1.1 depths by approximately 3 m. The central tropical Atlantic warm water thickness also shows occasional 10-m annual excursions of depth

(Fig. 9, bottom panel). Here thickness differences among analyses fall in the range of 2–3 m.

d. Arctic

The Arctic is a nearly closed basin whose exchanges with the other basins are limited to the subpolar North Atlantic and to a lesser extent the subpolar North Pacific. Because of the limited rate of exchange, the upper 50 m of the Arctic is capped by a highly stratified cool, fresh layer maintained by seasonal ice melting and river discharge (Fig. S6 shows a basinwide view and Fig. S7 shows the time-mean vertical structure at two locations). Beneath the halocline, at depths as shallow as 175 m, warm salty water of Atlantic origin is evident entering the central Arctic northward through Fram Strait and eastward across the Barents Sea Opening [discussed in Rudels et al. (2015) and Yashayaev and Seidov (2015)]. Hydrographic data coverage of this region peaked in the early 1980s, declined in the early 1990s, and has gradually recovered toward 1980 levels since then. More
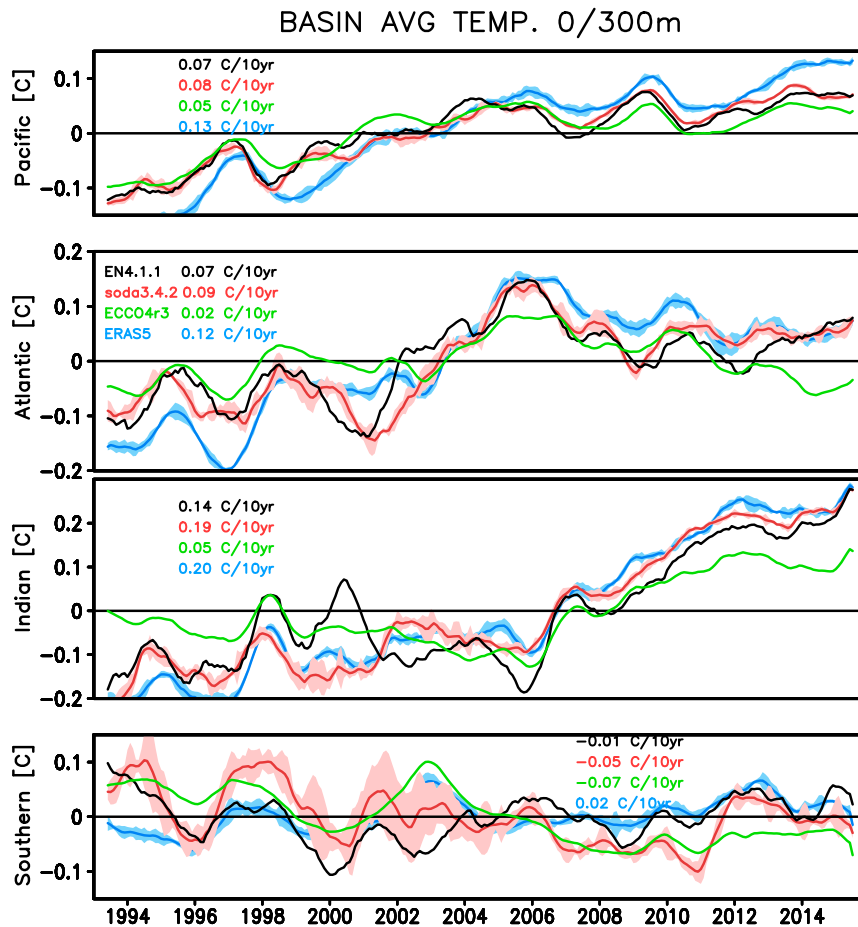
BASIN AVG TEMP. 0/300m

FIG. 7. Basin-average (70°S–60°N) shallow ocean temperature (°C) for 0–300 m over time for the four analyses for the (top to bottom) Pacific, Atlantic, Indian, and Southern Oceans. The series are identified in the Atlantic panel. Time series have been smoothed with a running 12-month filter. Basin domains are shown in Fig. S5. The linear trend for each ocean basin and each analysis is given in each panel. The ±1σ ensemble spreads are indicated in lighter shades.

information about the evolution of the Arctic observing system is provided in Zweng et al. (2018).

The salinity at the upper range of the Atlantic Water layer (200–250 m) shows that the reanalyses differ significantly in the ways in which this water mass is able to penetrate into the central Arctic (Fig. 10). The reanalyses show different extents of Atlantic Water spreading with SODA3 showing substantial amounts of Atlantic Water moving north and east through the 300-km-wide Fram Strait while the lower-resolution ECCO4r3 shows very little penetration and ORAS5 shows something in between (Fig. S7). In contrast to the Fram Strait, all three reanalyses show increasing water temperatures just east of the opening to the Barents Sea since the early 1990s, which is consistent with the movement of warming Atlantic Water crossing the Barents Sea Opening (Fig. 11).

South of the Fram Strait, Atlantic Water inflowing into the Greenland, Iceland, and Norwegian Seas shows

striking interannual variability (Polyakov et al. 2010; Carton et al. 2011; Beszczynska-Möller et al. 2012). The mid- to late 1990s, peaking in 1997, were characterized by generally cool and fresh conditions, while in the early 2000s (briefly in 1999–2000 and then more strongly in 2004–08) Atlantic Water underwent a dramatic 0.4°C surface-intensified warming. This strong variability of Atlantic Water properties appears in all four analyses (Fig. 12). Additionally, the reanalyses show another warm event beginning in 2014. The analyses also have significant differences, for example, regarding the strength of the surface-trapped warming in the early 2000s, but it is difficult to know which is more correct (Fig. 13).

On the Pacific side of the Arctic, the circulation of the Beaufort Sea (70.5°–80.5°N, 170°–130°W) also undergoes important interannual-to-decadal variations driven by changes in the strength of the Beaufort
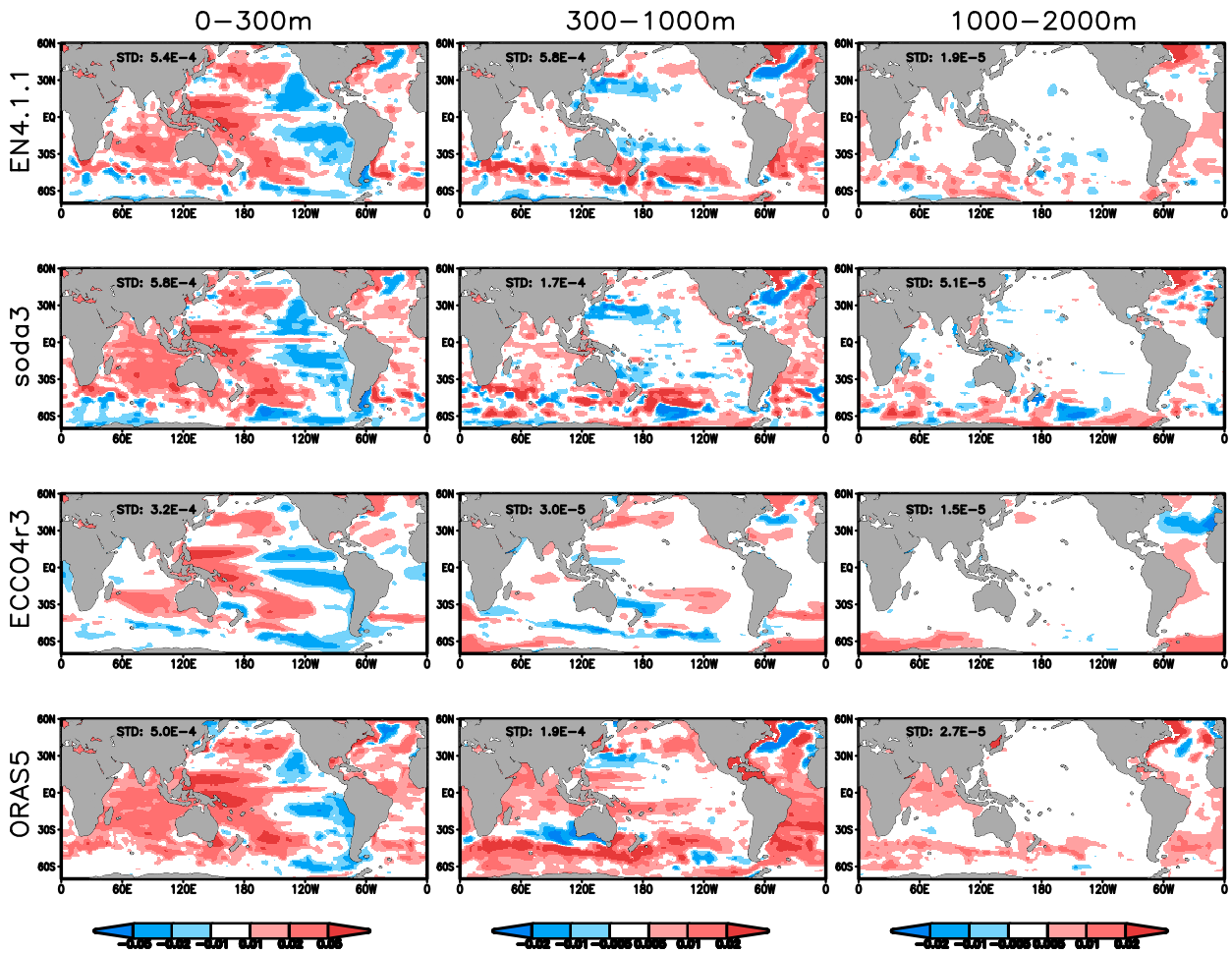
LAYER TEMPERATURE TREND

FIG. 8. Linear trend in layer-average analysis temperature (°C yr^{-1}) for 1993–2015 for (left) 0–300, (center) 300–1000, and (right) 1000–2000 m. The trend has been computed pointwise for each layer using least squares regression.

atmospheric surface high pressure system, the resulting anticyclonic surface winds, and the accumulation or discharge of near-surface freshwater (Fig. S7, bottom panels). The releases of freshwater accompanying a relaxation of the Beaufort Gyre have been implicated as a factor in the decadal climate variability of the subpolar North Atlantic (Proshutinsky et al. 2009).

Here we follow Proshutinsky et al. (2009) and define the liquid freshwater content (LFWC) of the gyre as the vertical integral in meters of the difference in salinity from a basin average $S_{ref} = 34.95$ psu:

$$\text{LFWC} = \int_{z\,(S=S_{ref})}^{0m} (1 - S/S_{ref})dz. \qquad (1.1)$$

The integral is taken down to a depth where the salinity equals the basin average (typically between 400 and 500 m). Intensive observations since 2003 show a

continuing accumulation of LFWC within the Beaufort Gyre (Fig. 14), which is also apparent in SODA3 and ORAS5. It is possible that the low storage rates of ECCO4r3 are affected by the fact that we carry out this analysis on a Mercator coordinate grid.

4. Summary and discussion

Early in this decade the international CLIVAR Global Synthesis and Observations Panel initiated a number of studies to evaluate available ocean reanalyses. Those extensive studies highlighted many common features such as a general agreement regarding displacements of the tropical Pacific and Indian Ocean thermoclines (also found in this study). For other phenomena, such as global ocean heat storage and variability at higher latitudes and deeper levels, there was much less agreement. In this study we extend the
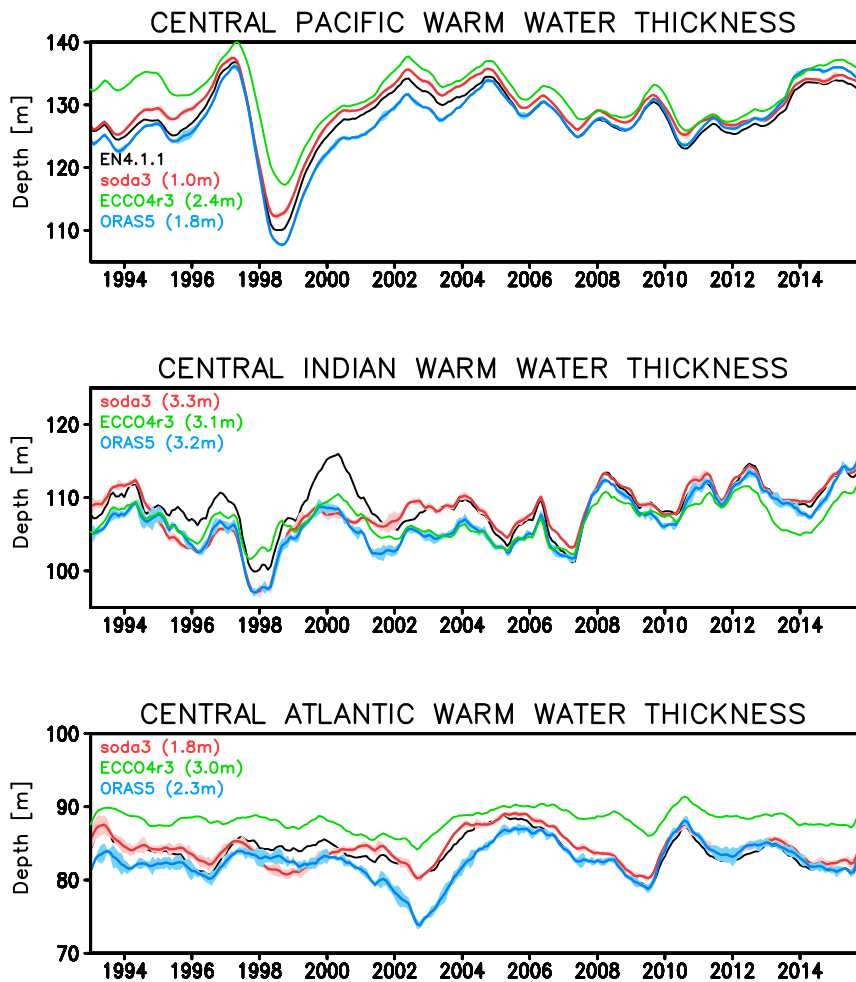
FIG. 9. Depth of the 20°C isotherm in the (top) central equatorial Pacific Ocean (8°S–8°N, 156°E–95°W), (middle) central equatorial Indian Ocean (8°S–8°N, 79°–90°E), and (bottom) central equatorial Atlantic Ocean (8°S–8°N, 30°–15°W). The time series have been smoothed with a running 12-month filter. The $\pm 1\sigma$ ensemble spreads are indicated in lighter shades. Standard deviations of the annual differences from EN4.1.1 are shown in parentheses.

evaluations to include several new ocean reanalyses: SODA3, ECCO4r3, and ORAS5 during their 23-yr period of overlap (1993–2015) to identify whether some of these previously noted differences have been resolved. Each uses a different model and assimilation algorithm, and somewhat different selections of constraining observations. ECCO4r3 and ORAS5 are forced by ERA-Interim surface forcing fields with some form of surface flux bias correction, while the SODA3 ensemble uses a variety of surface forcings including ERA-Interim. ORAS5 is also an ensemble reanalysis in which the ensemble members differ in parameter values and observation errors.

The present study began by directly comparing the reanalyses to observation-based SST and subsurface temperature and salinity analyses as well as by comparing to the historical database of profile observations.

Examination of the analysis-minus-observation misfits does show differences, including biases that are larger than what we might expect based on observation uncertainty. In many of these comparisons we include the EN4.1.1 statistical objective analysis, which has low bias by design since it is built around a climatological first guess. However, we also expect EN4.1.1 to have reduced accuracy compared to the reanalyses since the first guess lacks constraints associated with ocean dynamics and time-variable meteorology.

The three reanalyses all show slight mean differences from the widely cited OISSTv2 SST and EN4.1.1 analyses, with SODA3 and ORAS5 exhibiting a cool SST bias at southern latitudes and ECCO4r3 having a weak warm bias in the subtropics. Both SODA3 and ORAS5 are a bit saltier than EN4.1.1 in the Southern Hemisphere. In particular we note that the southern Pacific
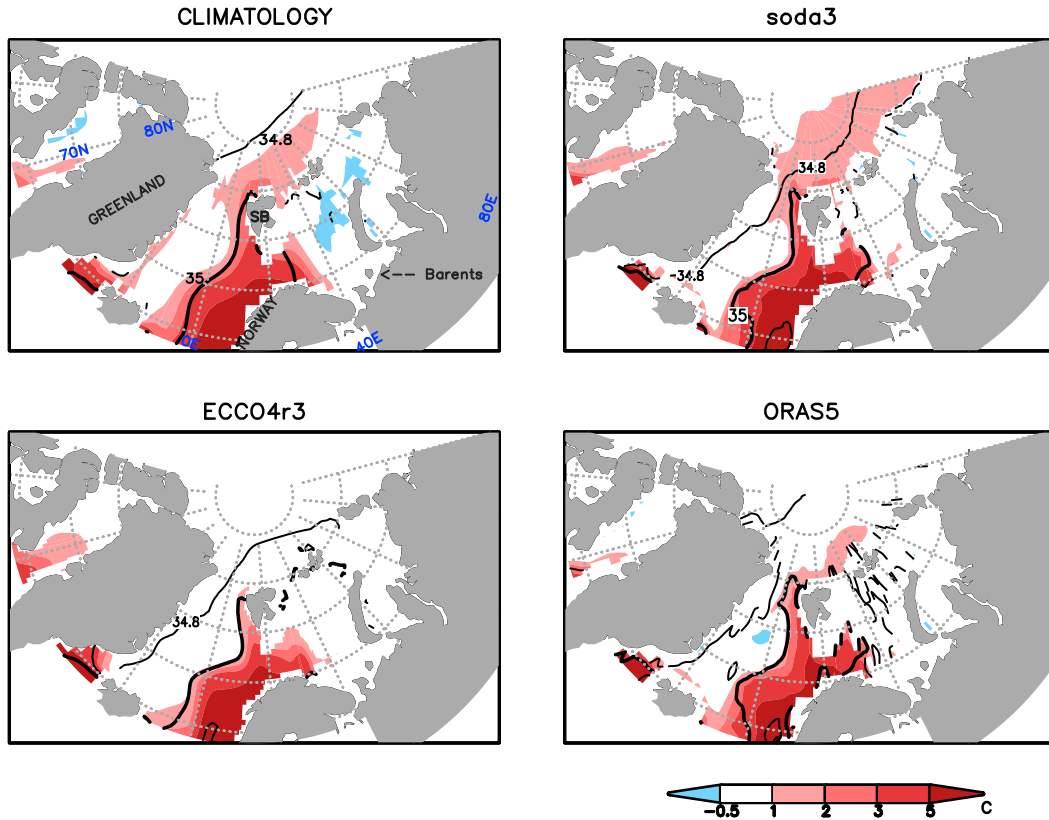
FIG. 10. Time-averaged Atlantic Water potential temperature (colors; °C) and salinity (contours; psu) in the Nordic seas and Arctic Ocean in the depth range of 200–250 m. Warm salty Atlantic Water enters the Arctic through the Fram Strait between Greenland and Spitsbergen (SB) and by crossing eastward into the Barents Sea Opening between Spitsbergen and Norway. (top left) PHC3.0 climatology, (top right) SODA3, (bottom left) ECCO4r3, and (bottom right) ORAS5.

subtropical near-surface high-salinity pool in ORAS5 and particularly SODA3 extends too far eastward in the 1980s and 1990s, a period when there are few constraining observations. All four analyses (EN4.1.1 and the three reanalyses) show very similar standard deviations of the analysis-minus-observation misfits. The presence of fronts and eddies ensures large errors of representation and thus eliminates the expectation of a

very close fit to the observations (Kalnay 2003; Janjić et al. 2018).

We next consider the global trends in temperature averaged into three depth layers: 0–300, 300–1000, and 1000–2000 m. Despite having similar spatial patterns, the global average trends still show differences among the three reanalyses. In the upper 300 m EN4.1.1 and SODA3 warm at a global average rate of 0.8°–0.09°C
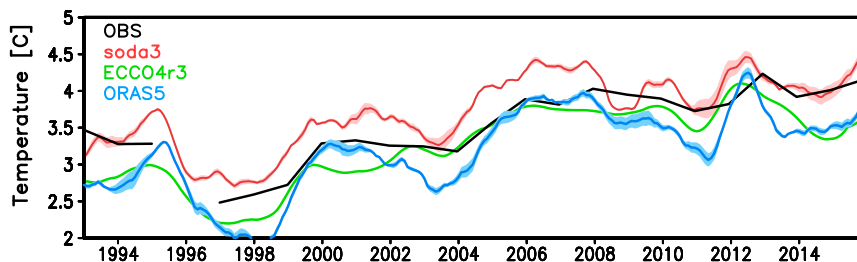

FIG. 11. Atlantic Water temperature (°C), averaged over 50–200 m, at the Barents Sea Opening (72°–73°N, 33.5°E). Observations (black) are from the Kola Meridian Transect (Matishov et al. 2009; Boitsov et al. 2012). Reanalysis time series have been smoothed with a 12-month running filter. The ±1σ ensemble spreads are indicated in lighter shades.

ATLANTIC WATER VARIABILITY

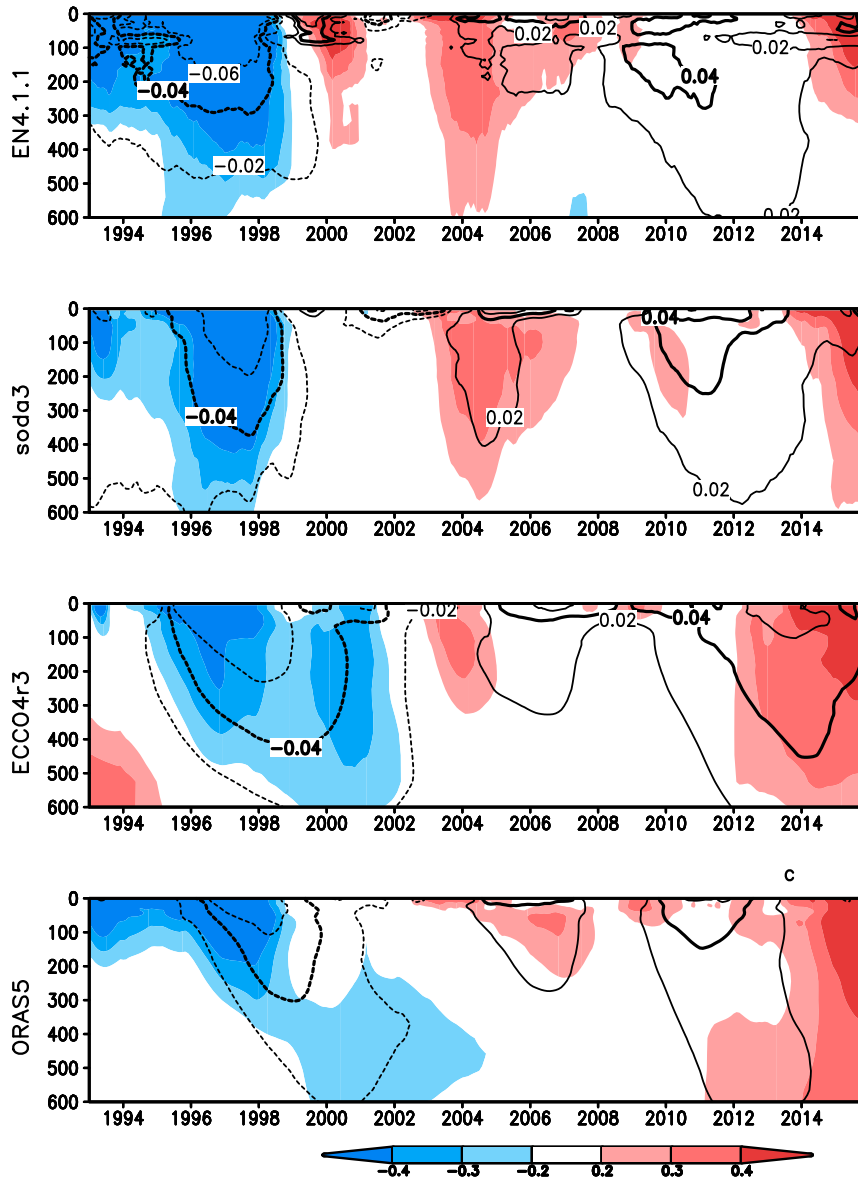FIG. 12. Anomaly from time-mean Atlantic Water potential temperature (colors; °C) and salinity (contours; psu) in the Greenland, Iceland, and Norwegian Seas as a function of depth and time. The Atlantic Water area is defined by the domain 65°–80°N, 15°W–18°E, where the time-mean salinity at 100-m depth exceeds 35 psu.

$(10\,\mathrm{yr})^{-1}$. In contrast, ORAS5 shows a stronger warming rate of $0.13°\mathrm{C}\ (10\,\mathrm{yr})^{-1}$, while ECCO4r3 has a much weaker warming rate of $0.04°\mathrm{C}\ (10\,\mathrm{yr})^{-1}$. Similar discrepancies exist in the deeper layers and in individual ocean basins. The lower rate of warming of ECCO4r3 than the others is particularly noticeable in the Indian Ocean, while the rates of warming of the reanalyses are most similar in the Pacific. All four analyses show little warming in the upper 300 m of the Southern Ocean.

Finally, in order to test the performance of the reanalyses at high latitudes, where the previous generation of reanalyses showed wide differences, we examine two types of Arctic climate variability: the changes in Atlantic Water properties in the Nordic seas on the Atlantic side and the changes in Beaufort Gyre freshwater storage on the Pacific side. The reanalyses show reassuringly similar Atlantic Water variability in the Greenland, Iceland, and Norwegian Seas, including the transition from cool and fresh conditions in the mid-1990s to warmer and saltier
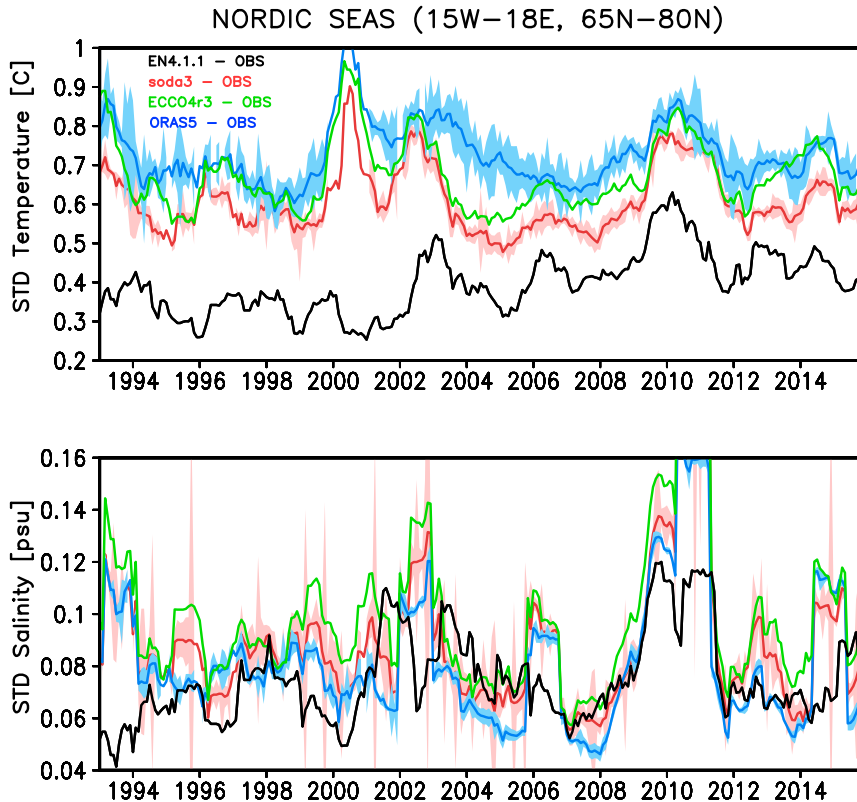
FIG. 13. Time series of annual average of the standard deviation of monthly 0–300-m analysis minus observations of (top) temperature and (bottom) salinity differences averaged over the domain 65°–80°N, 15°W–18°E, where the time-mean salinity at 100-m depth exceeds 35 psu. Colors show monthly $\pm1\sigma$ spreads of ensemble estimates.

conditions after 2000. However, there are differences in the representation of particular anomalous years, and also in the vertical structure of the anomalies and the correspondence between temperature and salinity variations, which we think are caused by differences in the pathways by which Atlantic Water enters the Arctic. On the Pacific side of the Arctic, both SODA3 and ORAS5 show increasing storage of freshwater with time at a rate similar to the observations.

In recent years ocean reanalyses have found wide application in studies of tropical interannual variability and we confirm their accuracy in reproducing interannual variability in the upper ocean. In contrast, ocean reanalyses have been applied less frequently for studies of decadal variability and at high latitude, and for studies of ocean heat uptake. The results presented here suggest that the levels of bias and the accuracy of representation of the historical observation set by the most recent
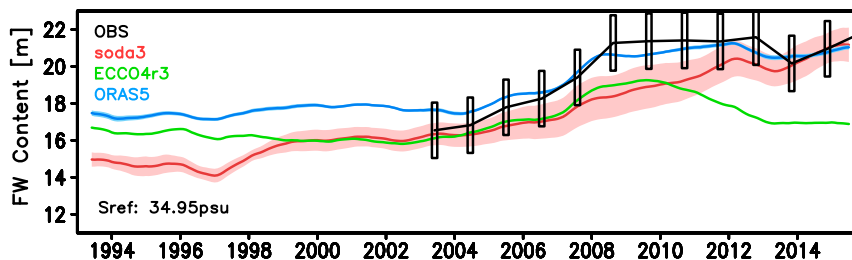

FIG. 14. Beaufort Gyre (70°–80°N, 170°–130°W) area-average liquid freshwater content (m) with time [see (1)]. Annual-average observation-based analysis of Proshutinsky et al. (2009) is shown in black. Corresponding reanalysis estimates have been computed using a reference salinity of 34.95 psu and have been smoothed with a 12-month running filter. The $\pm1\sigma$ ensemble spreads are indicated in lighter shades.

generation of ocean reanalyses is approaching that of the EN4.1.1 statistical objective analysis on basin scales, making them increasingly useful tools for a range of studies of decadal climate, including investigations of high-latitude variability. Also, the availability of multiple ensembles provides useful information about uncertainty. The global integrals of ocean heat uptake 1993–2015 still vary by an amount that exceeds the error estimates, suggesting there is still room for improvement. In particular we note that ECCO4r3 has somewhat weaker decadal variability and trends. On the other hand, this reanalysis has advantages for budget studies where conservation of heat and mass are crucial.

REFERENCES

Balmaseda, M. A., and Coauthors, 2015: The Ocean Reanalyses Intercomparison Project (ORA-IP). *J. Operational Oceanogr.*, **8** (S1), S80–S97, https://doi.org/10.1080/1755876X.2015.1022329.

Beszczynska-Möller, A., E. Fahrbach, U. Schauer, and E. Hansen, 2012: Variability in Atlantic water temperature and transport at the entrance to the Arctic Ocean, 1997–2010. *ICES J. Mar. Sci.*, **69**, 852–863, https://doi.org/10.1093/icesjms/fss056.

Boitsov, V. D., A. L. Karsakov, and A. G. Trofimov, 2012: Atlantic water temperature and climate in the Barents Sea, 2000–2009. *ICES J. Mar. Sci.*, **69**, 833–840, https://doi.org/10.1093/icesjms/fss075.

Boyer, T. P., and Coauthors, 2009: *World Ocean Database 2009*. S. Levitus, Ed., NOAA Atlas NESDIS 66, 216 pp. and DVDs.

Carton, J. A., B. S. Giese, and S. A. Grodsky, 2005: Sea level rise and the warming of the oceans in the Simple Ocean Data Assimilation (SODA) ocean reanalysis. *J. Geophys. Res.*, **110**, C09006, https://doi.org/10.1029/2004JC002817.

——, G. A. Chepurin, J. Reagan, and S. Hakkinen, 2011: Interannual to decadal variability of Atlantic Water in the Nordic and adjacent seas. *J. Geophys. Res.*, **116**, C11035, https://doi.org/10.1029/2011JC007102.

——, ——, and L. Chen, 2018a: SODA3: A new ocean climate reanalysis. *J. Climate*, **31**, 6967–6983, https://doi.org/10.1175/JCLI-D-18-0149.1.

——, ——, ——, and S. A. Grodsky, 2018b: Improved global net surface heat flux. *J. Geophys. Res. Oceans*, **123**, 3144–3163, https://doi.org/10.1002/2017JC013137.

Comiso, J., 2000 (updated 2015): Bootstrap sea ice concentrations for NIMBUS-7 SMMR and DMSP SSM/I. National Snow and Ice Data Center, https://doi.org/10.5067/J6JQLS9EJ5HU.

Dee, D. P., and Coauthors, 2011: The ERA-Interim reanalysis: Configuration and performance of the data assimilation system. *Quart. J. Roy. Meteor. Soc.*, **137**, 553–597, https://doi.org/10.1002/qj.828.

Domingues, C. M., J. A. Church, N. J. White, P. J. Gleckler, S. E. Wijffels, P. M. Barker, and J. R. Dunn, 2008: Improved estimates of upper-ocean warming and multi-decadal sea-level rise. *Nature*, **453**, 1090–1093, https://doi.org/10.1038/nature07080.

Donlon, C. J., M. Martin, J. Stark, J. Roberts-Jones, E. Fiedler, and W. Wimmer, 2012: The Operational Sea Surface Temperature and Sea Ice Analysis (OSTIA) system. *Remote Sens. Environ.*, **116**, 140–158, https://doi.org/10.1016/j.rse.2010.10.017.

Dussin, R., B. Barneir, L. Brodeau, and J. M. Molines, 2016: The making of the DRAKKAR forcing set DFS5. DRAKKAR/MyOcean Report 01-04-16, 34 pp., https://www.drakkar-ocean.eu/publications/reports/report_DFS5v3_April2016.pdf.

Forget, G., J.-M. Campin, P. Heimbach, C. N. Hill, R. M. Ponte, and C. Wunsch, 2015: ECCO version 4: An integrated framework for non-linear inverse modeling and global ocean state estimation. *Geosci. Model Dev.*, **8**, 3071–3104, https://doi.org/10.5194/gmd-8-3071-2015.

Fukumori, I., O. Wang, I. Fenty, G. Forget, P. Heimbach, and R. M. Ponte, 2017: ECCO Version 4 Release 3. 10 pp., ftp://ecco.jpl.nasa.gov/Version4/Release3/doc/v4r3_estimation_synopsis.pdf.

Gelaro, R., and Coauthors, 2017: The Modern-Era Retrospective Analysis for Research and Applications, version 2 (MERRA-2). *J. Climate*, **30**, 5419–5454, https://doi.org/10.1175/JCLI-D-16-0758.1.

Good, S. A., M. J. Martin, and N. A. Rayner, 2013: EN4: Quality controlled ocean temperature and salinity profiles and monthly objective analyses with uncertainty estimates. *J. Geophys. Res.*, **118**, 6704–6716, https://doi.org/10.1002/2013JC009067.

Gouretski, V., and F. Reseghetti, 2010: On depth and temperature biases in bathythermograph data: development of a new correction scheme based on analysis of a global database. *Deep-Sea Res. I*, **57**, 812–833, https://doi.org/10.1016/j.dsr.2010.03.011.

Han, W., J. Vialard, M. J. McPhaden, T. Lee, Y. Masumoto, M. Feng, and W. P. de Ruijter, 2014: Indian Ocean decadal variability: A review. *Bull. Amer. Meteor. Soc.*, **95**, 1679–1703, https://doi.org/10.1175/BAMS-D-13-00028.1.

Janjić, T., and Coauthors, 2018: On the representation error in data assimilation. *Quart. J. Roy. Meteor. Soc.*, **144**, 1257–1278, https://doi.org/10.1002/qj.3130.

Kalnay, E., 2003: *Atmospheric Modeling, Data Assimilation and Predictability*. Cambridge University Press, 341 pp.

Karspeck, A. R., and Coauthors, 2017: Comparison of the Atlantic meridional overturning circulation between 1960 and 2007 in six ocean reanalysis products. *Climate Dyn.*, **49**, 957–982, https://doi.org/10.1007/s00382-015-2787-7.

Kobayashi, S., and Coauthors, 2015: The JRA-55 Reanalysis: General specifications and basic characteristics. *J. Meteor. Soc. Japan*, **93**, 5–48, https://doi.org/10.2151/jmsj.2015-001.

Lee, S.-K., W. Park, M. O. Baringer, A. L. Gordon, B. Huber, and Y. Liu, 2015: Pacific origin of the abrupt increase in Indian Ocean heat content during the warming hiatus. *Nat. Geosci.*, **8**, 445–449, https://doi.org/10.1038/ngeo2438.

Levitus, S., J. I. Antonov, T. Boyer, R. A. Locamini, H. E. Garcia, and A. V. Mishonov, 2009: Global ocean heat content 1955–2008 in light of recently revealed instrumentation problems. *Geophys. Res. Lett.*, **36**, L07608, https://doi.org/10.1029/2008GL037155.

Liang, X., and L. Yu, 2016: Variations of the global net air–sea heat flux during the "hiatus" period (2001–10). *J. Climate*, **29**, 3647–3660, https://doi.org/10.1175/JCLI-D-15-0626.1.

Lyman, J. M., and G. C. Johnson, 2014: Estimating global ocean heat content changes in the upper 1800 m since 1950 and the influence of climatology choice. *J. Climate*, **27**, 1945–1957, https://doi.org/10.1175/JCLI-D-12-00752.1.

Matishov, G. G., D. G. Matishov, and D. V. Moiseev, 2009: Inflow of Atlantic-origin waters to the Barents Sea along glacial troughs. *Oceanologia*, **51**, 321–340, https://doi.org/10.5697/oc.51-3.321.

Meinen, C. S., and M. J. McPhaden, 2001: Interannual variability in warm water volume transports in the equatorial Pacific during 1993–99. *J. Phys. Oceanogr.*, **31**, 1324–1345, https://doi.org/10.1175/1520-0485(2001)031<1324:IVIWWV>2.0.CO;2.

Nieves, V., J. K. Willis, and W. C. Patzert, 2015: Recent hiatus caused by decadal shift in Indo-Pacific heating. *Science*, **349**, 532–535, https://doi.org/10.1126/science.aaa4521.

Palmer, M. D., and Coauthors, 2017: Ocean heat content variability and change in an ensemble of ocean reanalyses. *Climate Dyn.*, **49**, 909–930, https://doi.org/10.1007/s00382-015-2801-0.

Polyakov, I. V., and Coauthors, 2010: Arctic Ocean warming contributes to reduced polar ice cap. *J. Phys. Oceanogr.*, **40**, 2743–2756, https://doi.org/10.1175/2010JPO4339.1.

Proshutinsky, A., and Coauthors, 2009: Beaufort Gyre freshwater reservoir: State and variability from observations. *J. Geophys. Res.*, **114**, C00A10, https://doi.org/10.1029/2008JC005104.

Reiniger, R. F., and C. K. Ross, 1968: A method for interpolation with application to oceanographic data. *Deep-Sea Res.*, **15**, 185–193, https://doi.org/10.1016/0011-7471(68)90040-5.

Reynolds, R. W., N. A. Rayner, T. M. Smith, D. C. Stokes, and W. Wang, 2002: An improved in situ and satellite SST analysis for climate. *J. Climate*, **15**, 1609–1625, https://doi.org/10.1175/1520-0442(2002)015<1609:AIISAS>2.0.CO;2.

——, T. M. Smith, C. Liu, D. B. Chelton, K. S. Casey, and M. G. Schlax, 2007: Daily high-resolution blended analyses for sea surface temperature. *J. Climate*, **20**, 5473–5496, https://doi.org/10.1175/2007JCLI1824.1.

Rhein, M., and Coauthors, 2013: Observations: Ocean. *Climate Change 2013: The Physical Science Basis*, T. F. Stocker et al., Eds., Cambridge University Press, 255–315.

Rudels B., M. Korhonen, U. Schauer, S. Pisarev, B. Rabe, and A. Wisotzki, 2015: Circulation and transformation of Atlantic water in the Eurasian Basin and the contribution of the Fram Strait inflow branch to the Arctic Ocean heat budget. *Prog. Oceanogr.*, **132**, 128–152, https://doi.org/10.1016/j.pocean.2014.04.003.

Saji, N. H., B. N. Goswami, P. N. Vinayachandran, and T. Yamagata, 1999: A dipole mode in the tropical Indian Ocean. *Nature*, **401**, 360–363.

Schulzweida, U., 2018: CDO User Guide: Climate Data Operator version 1.9.4. Max-Planck Institute for Meteorology, 216 pp., https://code.mpimet.mpg.de/projects/cdo/embedded/cdo.pdf.

Shi, L., and Coauthors, 2017: An assessment of upper ocean salinity content from the Ocean Reanalyses Intercomparison Project (ORA-IP). *Climate Dyn.*, **49**, 1009–1029, https://doi.org/10.1007/s00382-015-2868-7.

Smolyar, D., and M. M. Zweng, 2013: *World Ocean Database 2013*. S. Levitus, Ed., NOAA Atlas NESDIS 72, 209 pp.

Steele, M., R. Morley, and W. Ermold, 2001: PHC: A global ocean hydrography with a high-quality Arctic Ocean. *J. Climate*, **14**, 2079–2087, https://doi.org/10.1175/1520-0442(2001)014<2079:PAGOHW>2.0.CO;2.

Storto, A., and Coauthors, 2017: Steric sea level variability (1993–2010) in an ensemble of ocean reanalyses and objective analyses. *Climate Dyn.*, **49**, 709–729, https://doi.org/10.1007/s00382-015-2554-9.

Toyoda, T., and Coauthors, 2017a: Intercomparison and validation of the mixed layer depth fields of global ocean syntheses. *Climate Dyn.*, **49**, 753–773, https://doi.org/10.1007/s00382-015-2637-7.

——, and Coauthors, 2017b: Interannual-decadal variability of wintertime mixed layer depths in the North Pacific detected by an ensemble of ocean syntheses. *Climate Dyn.*, **49**, 891–907, https://doi.org/10.1007/s00382-015-2762-3.

Trenberth, K. E., J. T. Fasullo, K. von Schuckmann, and L. Cheng, 2016: Insights into Earth's energy imbalance from multiple sources. *J. Climate*, **29**, 7495–7505, https://doi.org/10.1175/JCLI-D-16-0339.1.

Valdivieso, M., and Coauthors, 2017: An assessment of air–sea heat fluxes from ocean and coupled reanalyses. *Climate Dyn.*, **49**, 983–1008, https://doi.org/10.1007/s00382-015-2843-3.

Wong, A. P. S., and G. C. Johnson, 2003: South Pacific Eastern Subtropical Mode Water. *J. Phys. Oceanogr.*, **33**, 1493–1509, https://doi.org/10.1175/1520-0485(2003)033<1493:SPESMW>2.0.CO;2.

Yashayaev, I., and D. Seidov, 2015: The role of the Atlantic Water in multidecadal ocean variability in the Nordic and Barents Seas. *Prog. Oceanogr.*, **132**, 68–127, https://doi.org/10.1016/j.pocean.2014.11.009.

Zuo, H., M. Balmaseda, E. de Boisseson, S. Hirahara, M. Chrust, and P. de Rosnay, 2017: A generic ensemble generation scheme for data assimilation and ocean analysis. ECMWF Tech. Memo. **795**, 44 pp., https://doi.org/10.21957/cub7mq0i4.

——, ——, S. Tietsche, K. Mogensen, and M. Mayer, 2019: The ECMWF operational ensemble reanalysis-analysis system for ocean and sea-ice: A description of the system and assessment. *Ocean Sci. Discuss.*, https://doi.org/10.5194/os-2018-154.

Zweng, M. M., T. P. Boyer, O. K. Baranova, J. R. Reagan, D. Seidov, and I. V. Smolyar, 2018: An inventory of Arctic Ocean data in the World Ocean Database. *Earth Syst. Sci. Data*, **10**, 677–687, https://doi.org/10.5194/essd-10-677-2018.